DOI: 10.26599/FSHW.2026.9250993

Contents lists available at SciOpen

Food Science and Human Wellness

journal homepage: https://www.sciopen.com/journal/2097-0765

China Food Publishing Co.

Garlic-Derived Exosome-Like Nanovesicles Mitigate Acute Lung Injury via Blocking Activation of the cGAS-STING Signaling to Reduce Inflammatory Response

Siyuan Zhang [a,1], Xu Wang [a,1], Tianyuan Wang [a,1], Diaodiao Liu [a], Ran Li [a,1], Songsong Jing [b], Chunlin Zhuang [a, c*], Zhuo Qu [a*]

[a] *Key Laboratory of Protection, Development and Utilization of Medicinal Resources in Liupanshan Area, Ministry of Education, College of Pharmacy, Ningxia Medical University, 1160 Shengli Street, Yinchuan, Ningxia 750004, China*

[b] *Traditional Chinese Medicine Processing Technology Innovation Centre of Hebei Province, College of Pharmacy, Hebei University of Chinese Medicine, Shijiazhuang, 050200, China*

[c] *School of Pharmacy, Naval Medical University, 325 Guohe Road, Shanghai 200433, China*

ABSTRACT: Acute lung injury (ALI) is a life-threatening disorder featured by pulmonary inflammation, with no highly effective pharmacological treatments available. Given the anti-inflammatory property of garlic (*Allium sativum* L.) and the therapeutic potential of plant-derived nanovesicles, we hypothesized garlic-derived exosome-like nanovesicles (GAELNs) protect against ALI. In our present study, GAELNs were successfully isolated, purified, and characterized, showing typical exosomal traits and diverse biomolecules. *In vivo*, GAELNs administration mitigated LPS-induced lung histopathological damage and suppressed pro-inflammatory cytokine production. *In vitro*, GAELNs were efficiently internalized by RAW264.7 macrophages, leading to reduced secretion of harmful cytokines. Transcriptomic profiling indicated that the anti-ALI effects of GAELNs were associated with modulation of multiple inflammatory signaling pathways. Mechanistically, GAELNs conferred protection by potently inhibiting the cGAS-STING signaling axis and its downstream effectors. Collectively, GAELNs alleviate ALI by inhibiting the cGAS-STING mediated inflammatory cascade, representing a promising novel therapeutic strategy for ALI.

Keywords: Garlic-derived exosome-like nanovesicles; Acute lung injury; cGAS-STING signaling; Inflammatory response

1. Introduction

Acute lung injury (ALI) is a severe inflammatory disorder associated with alveolar damage, macrophage activation, inflammatory cell infiltration, and cytokine production [1]. It is characterized by decreased lung compliance, severe hypoxemia, and progressive hypoxic respiratory failure resulting from various pulmonary and systemic insults, including infections, chemical exposures, and mechanical trauma [2, 3]. Despite advances in medical technology and therapeutic strategies, the mortality rate of ALI is over 40% [4, 5]. Currently, there is no cure or FDA-approved therapy for ALI [6]. Existing pharmacological

[1] These authors contributed equally.
***Corresponding author**
zclnathan@163.com (C. Zhuang), quzhuo2008@163.com (Z. Qu).

Received 1 September 2025
Received in revised from 8 October 2025
Accepted 29 October 2025

interventions remain limited, primarily relying on antibiotics and glucocorticoids, which often produce serious adverse reactions [3]. Therefore, the development of novel therapeutic agents with specific anti-inflammatory properties is critical for improving clinical outcomes in ALI patients. Current evidence suggests that systemic inflammatory responses following infections or trauma serve as the fundamental pathogenic mechanism underlying ALI [7]. Effective management of primary pathological foci and interruption of the ensuing dysregulated systemic inflammatory cascade are therefore considered pivotal for both prevention and treatment of ALI [7]. In recent years, the discovery of safe and effective anti-ALI compounds derived from natural plants has emerged as a significant research focus, offering potential alternatives and adjunctive therapeutics to conventional pharmacological approaches.

Cell-derived nanovesicles (NVs), characterized by nanosized membranous structures, serve as carriers for bioactive molecules such as nucleic acids, proteins, lipids, and metabolites. These NVs regulate physiological functions in organisms through cross-species transfer of biological information [8-10]. In recent years, mammalian-derived NVs have demonstrated broad application prospects in biomedical fields, including drug delivery, disease diagnosis, and tissue regeneration [10-12]. It is noteworthy that, as one of the main active parts of plants, plant-derived NVs (PDNVs) have gained significant attention due to the advantages of biocompatibility, cost-effectiveness, environmental sustainability, and scalability for mass production [13, 14]. Research has revealed that PDNVs not only modulate plant innate immunity via intercellular communication but also mediate cross-species small RNA interference to induce gene silencing in fungal pathogens [15, 16]. Furthermore, bioactive components encapsulated within PDNVs have exhibited therapeutic potential through oral administration or tail vein injection. Notably, several PDNVs, such as those from Platycodon grandiflorus [17], Artemisia annua [18], and Ginger [19], have demonstrated alleviative effects on ALI, highlighting the potential advantages of PDNVs in mitigating ALI.

Garlic (*Allium sativum* L.), a member of the *Liliaceae* family, is a widely recognized medicinal and edible plant with a long history. For centuries, it has served not only as an indispensable culinary spice but also as a medicinal plant for disease prevention and treatment [20]. Garlic is rich in diverse bioactive compounds, among which organosulfur derivatives are considered the most characteristic active constituents [21]. Recently, we have demonstrated that garlic oil and its primary organosulfur compounds, diallyl disulfide (DADS) and diallyl trisulfide (DATS), exhibit significant inhibitory effects on tobacco carcinogen 4-(Methylnitrosamino)-1-(3-pyridyl)-1-butanone (NNK)-induced pulmonary inflammation [22-24]. Additionally, the anti-inflammatory properties of other components derived from garlic have been extensively documented. For instance, diallyl sulfide (DAS) has been reported to inhibit high NF-κB protein expression, as well as the expression of cyclooxygenase-2 (COX-2), prostaglandin E2 (PGE2), tumor necrosis factor α (TNF-α), interleukin 1β (IL-1β), and interleukin 6 (IL-6) genes, and to reduce reactive oxygen species (ROS) production [25]. S-allylcysteine (SAC) inhibits nitric oxide (NO) production by suppressing TNF-α and inducible nitric oxide synthase (iNOS) mRNA and protein expression, as well as NF-κB activation [26], modulate the AKT/NF-κB signaling pathway to prevent lung fibrosis induced by bleomycin [27], and reduces

allergic airway inflammation and mucus production in ovalbumin-induced asthmatic mice [28]. The anti-inflammatory properties of allicin have also been shown to protect against ALI. Wang and colleagues discovered that allicin can reduce lipopolysaccharide (LPS)-induced NF-κB activation and inflammatory responses by activating peroxisome proliferator activated receptor γ (PPARγ) [29]. Collectively, these findings underscore the nutritional richness and robust bioactivity of garlic, positioning it as an excellent source for isolating exosome-like nanovesicles from plants. Indeed, several research groups have successfully isolated garlic-derived exosome-like nanovesicles (GAELNs) and investigated their therapeutic potential. Studies reveal that GAELNs ameliorates pathological conditions such as high-fat diet-induced obesity [30, 31], colitis [32, 33], acute liver failure [34, 35], and type II diabetes [36], while enhancing cancer immunotherapy efficacy [37]. Specifically, GAELNs alleviates dextran sulfate sodium-induced mouse colitis via the TLR4/MyD88/NF-κB signaling pathway [32]. Furthermore, GAELNs protects against hepatic injury by suppressing CCR2/CCR5 signaling and mitigating inflammatory bursts [34]. Based on these evidence, we reasonably hypothesize that GAELNs has the ability to alleviate ALI. To verify this hypothesis, GAELNs were isolated from fresh garlic using ultracentrifugation combined with sucrose density gradient centrifugation, followed by compositional characterization. The anti-inflammatory activity and underlying mechanisms of GAELNs were systematically investigated using LPS-induced inflammatory models in RAW264.7 macrophages and mouse ALI models. The successful implementation of this study will clarify the mitigation effect of GAELNs on LPS-induced ALI and reveal its potential mechanism of action, thereby laying an experimental foundation for GAELNs to be used in the prevention and treatment of ALI.

2. Materials and Methods

2.1. Chemicals and reagents

The chemical reagents and materials were sourced as follows: LPS (purity > 98%) was obtained from Solarbio Technology Co., Ltd. (Beijing, China). Enzyme-linked immunosorbent assay (ELISA) kits for IL-1β, TNF-α, and IL-6 quantification were purchased from MultiSciences (Lianke) Biotech Co., Ltd. (Hangzhou, China). For western blot analysis, the following antibodies were employed: anti-NF-κB p65 antibody (p65, 1:1000, Proteintech, Catalogue numbers: 10745-1-AP), anti-phospho-NF-κB p65 (Ser536) (p-p65, 1:1000, Proteintech, Catalogue numbers: 39675), anti-IκBα antibody (IκBα, 1:5000, Proteintech, Catalogue numbers: 18220-1-AP), anti-phospho-IκBα antibody (p-IκBα, 1:1000, Proteintech, Catalogue numbers: 82349-1-RR), anti-TNF-α antibody (TNF-α, 1:1000, Proteintech, Catalogue numbers: 17590-1-AP), Anti-IL-6 antibody (IL-6, 1:500, Proteintech, Catalogue numbers: 11764-1-AP), anti-IL-1β antibody (IL-1β, 1:1000, Proteintech, Catalogue numbers: 16806-1-AP), anti-cGAS antibody (cGAS, 1:1000, Proteintech, Catalogue numbers: 16806-1-AP), anti-STING antibody (STING, 1:1000, Proteintech, Catalogue numbers: 19851-1AP), anti-TBK1 antibody (TBK1, 1:2000, Biodragon, Catalogue numbers: RM1235), anti-phospho-TBK1 antibody (p-TBK1, 1:500, Affinity Biosciences, Catalogue numbers: AF8190), anti-IRF3 antibody (IRF3, 1:5000, Proteintech, Catalogue numbers: 66670-1-lg), anti-phospho-IRF3 antibody (p-IRF3, 1:1000, Biodragon, Catalogue numbers: BD-PP0326), anti-MLKL antibody (MLKL, 1:1000, Proteintech, Catalogue

numbers: 21066-1-AP), anti-phospho-MLKL antibody (p-MLKL, 1:1000, Biodragon, Catalogue numbers: RM2661), anti-lamin B1 antibody (Lamin B1, 1:5000, Proteintech, Catalogue numbers:12987-1-AP), anti β-actin antibody (β-actin, 1:5000, Proteintech, Catalogue numbers: 20536-1-AP), anti GAPDH antibody (GAPDH, 1:5000, Proteintech, Catalogue numbers: 10494-1-AP), and goat antirabbit IgG (IgG, 1:5000, Proteintech, Catalogue numbers: SA00001-2). Primers were sourced from Sangon Biotech Co., Ltd. (Shanghai, China).

2.2. Isolation and purification of GAELNs

Fresh garlic bulbs were obtained locally, washed three times with 1× PBS, and homogenized in precold PBS (4°C) using a blender. The collected juice underwent a multi-step centrifugation procedure and outlined in Fig. 1A. Briefly, sequential centrifugation was performed at 2,000 g (20 min), 3,500 g (40 min), 5,000 g (40 min), and 10,000 g (40 min) to remove cellular debris. The supernatant was then subjected to ultracentrifugation at 150,000 g for 2 h. The resulting pellet was resuspended in sterile PBS and layered onto a discontinuous sucrose gradient (8%, 15%, 30%, 45%, 60%). Following centrifugation at 150,000 g for 2 h (4°C), the band at the 30% ~ 45% sucrose interface was collected, yielding GAELNs. To remove residual sucrose, the collected GAELNs fraction was diluted in PBS, pelleted by ultracentrifugation (150,000 g, 2 h), resuspended in PBS, and stored at -80°C.

GAELNs morphology was assessed by transmission electron microscopy (TEM, HT-7800, Hitachi High-Tech). Particle size distribution was determined using dynamic light scattering (DLS) and confirmed by TEM. Surface charge (Zeta potential) was measured using a Malvern Zetasizer Nano ZS90 instrument (Malvern Instruments Ltd., UK).

2.3. Metabolomic analysis of GAELNs

Metabolites of GAELNs were analyzed by LC-MS/MS using a Vanquish UHPLC system (Thermo Fisher Scientific) equipped with a Phenomenex Kinetex C18 column (2.1 mm × 50 mm, 2.6 μm) and coupled to an Orbitrap Exploris 120 mass spectrometer (Thermo Fisher Scientific). Chromatographic separation employed: mobile phase A (0.01% acetic acid in water) and B [isopropanol:acetonitrile (1:1, v/v)], column temperature 25°C, auto-sampler temperature 4°C, and injection volume 2 μL. Mass spectrometric data were acquired in information-dependent acquisition (IDA) mode via Xcalibur software (Thermo), enabling continuous full MS scans with triggered MS/MS. ESI source parameters included: sheath/auxiliary/sweep gas flows at 50/15/1 Arb, capillary/vaporizer temperatures at 320/350°C, full MS/MS resolutions of 60,000/15,000, stepped NCE (20/30/40 eV), and spray voltages of ± 3.8 kV (positive) or -3.4 kV (negative). Raw data were converted to mzXML using ProteoWizard, processed through an in-house R script (XCMS-based) for peak detection/extraction/alignment/integration, and metabolites identified via R packages with BiotreeDB v3.0.

2.4. Lipidomic analysis of GAELNs

Lipid analysis was conducted via LC-MS/MS using a Vanquish UHPLC system (Thermo Fisher Scientific) coupled to an Orbitrap Exploris 120 mass spectrometer (Thermo), equipped with a Phenomenex Kinetex C18 column (2.1 mm × 100 mm, 2.6 μm). Chromatographic conditions comprised: mobile phase A [H_2O/acetonitrile (6:4, v/v) with 10 mM $HCOONH_4$], mobile phase B [isopropanol/acetonitrile (9:1, v/v) with 10 mM $HCOONH_4$], and 2 μL injection volume. Mass spectrometric data acquisition in IDA mode was controlled by Xcalibur software (Thermo), enabling continuous full MS scans with triggered MS/MS. ESI parameters included: sheath/auxiliary gas flows at 30/10 Arb, capillary temperature 320°C, full MS/MS resolutions of 60,000/15,000, stepped NCE (15/30/45 eV), and spray voltages of ± 3.8 kV (positive) or -3.4 kV (negative). Raw data were converted to mzXML via ProteoWizard's msconvert, processed using XCMS' CentWave algorithm for peak detection/extraction/alignment/integration (minfrac = 0.5, cutoff = 0.3), with lipid identification achieved through spectral matching against the LipidBlast library.

2.5. Proteomic analysis of GAELNs

Peptide samples were prepared through protein extraction, BCA quantification, reduction/alkylation, and digestion, followed by NanoDrop peptide quantification. For analysis, 200 ng peptides per sample were separated on a nano-UPLC system (Evosep One) coupled to a timsTOF Pro2 mass spectrometer (Bruker) via nano-ESI. Chromatographic separation used a PepSep C18 column (1.9 μm, 150 μm × 15 cm, Bruker, Germany) with mobile phases: A (0.1% formic acid in H_2O) and B (0.1% formic acid in acetonitrile). Mass spectrometry employed data-dependent acquisition (DDA) with PaSFF mode, scanning m/z 100-1700 (MS1). During PASEF MS/MS, collision energy ramped linearly with ion mobility from 20 eV ($1/K_0$ = 0.6 Vs/cm^2) to 59 eV ($1/K_0$ = 1.6 Vs/cm^2). Raw files were processed in SpectroMine (v4.2.230428.52329) using label-free quantitation (LFQ).

2.6. miRNA profiling of GAELNs

RNA preparation, library construction, and sequencing were outsourced to Baiqu Biomedical Technology Co., Ltd. (Shanghai, China). Total RNA from GAELNs was extracted using TRIzol reagent (Invitrogen), followed by small RNA library preparation with the TruSeq Small RNA Kit (Illumina). Libraries underwent 50-cycle single-end sequencing on an Illumina HiSeq 2500 platform. Raw reads were processed through ACGT101_miR v4.2 (LC Sciences) for quality/adapter trimming and size selection, with subsequent miRNA functional annotation via Blast2GO and KEGG databases.

2.7. Cell culture

The RAW264.7 cell line was obtained from the National Collection of Authenticated Cell Cultures (Shanghai, China). These cells were cultured in basic culture medium supplemented with 10% (v/v) fetal bovine serum and 1% (v/v) penicillin/streptomycin. The cells were maintained in a 37°C incubator with 5% CO_2 atmosphere, with the cell culture medium replaced on a daily basis. When the cells grew to 90%, 0.25% trypsin was used for digestion and passage.

2.8. Cytotoxicity assay

Cell viability was assessed using the Cell Counting Kit-8 (CCK-8) assay. RAW264.7 cells were seeded at a density of 4×10^4 cells/well in 96-well plates. After 24 h, the cells were exposed to GAELNs at the concentrations of 0, 0.0742, 0.148, 0.297, 0.594, 1.18, 2.37, 4.75, and 9.5 mg/mL, respectively. At 24 h post-treatment, the CCK-8 reagent was added to the cells, and the plates were incubated at 37°C for 4 h. The optical density (OD) values were then measured using a microplate reader.

2.9. Construction of acute cell injury model and intervention with GAELNs

RAW264.7 macrophages were divided into the Control group, LPS group and LPS+GAELNs group. The macrophages in each group were inoculated in 6-well plates at the density of 3×10^5 cells/well and cultured for 24 h. Then, the LPS group and LPS+GAELNs group were added with 1 μg/mL LPS, while the LPS+GAELNs group was added with both 1 μg/mL LPS and GAELNs at the concentrations of 0, 0.0371, 0.0742, 0.148, 0.297, 0.594 mg/mLfor intervention for 24 h, respectively.

2.10. Determination of NO by Griess assay

RAW 264.7 cells were seeded in 96-well plates at 3×10^5 cells/well for 24 h. To establish an inflammatory model, cells were treated with both 1 μg/mL LPS and GAELNs at the concentrations of 0.594 mg/mL for 24 h at 37°C. Nitric oxide content in culture supernatants was quantified using a Total Nitric Oxide Assay Kit (Beyotime Biotechnology, China) per manufacturer's protocol. Absorbance at 540 nm was measured on a Multiskan GO microplate reader, with concentrations calculated against a $NaNO_2$ standard curve.

2.11. Determination of cellular ROS

Intracellular ROS levels were measured using 2,7-Dichlorofluorescin Diacetate (DCFH-DA), a cell-permeable fluorescent probe provided by Nanjin Jiancheng Bioengineering Institute (Nanjin, China). Following the 24-h treatment with LPS 1 μg/mL or a combination of LPS and GAELNs0.594 mg/mL, the cells were incubated with 10 μM DCFH-DA for 30 min at 37°C, washed with PBS, and analyzed for green fluorescence intensity using a fluorescence microplate reader.

2.12. Determination of cellular GSH

Intracellular glutathione (GSH) levels were quantified using commercial assay kits provided by the Nanjing Jiancheng Bioengineering Institute (Nanjing, China). RAW 264.7 macrophages were treated as described in section 2.11. After the 24 h treatment period, cells were collected, lysed, and centrifuged. The resulting supernatants were used for the assay. The measurements were performed according to the protocols recommended by the manufacturer, with absorbance measurements determined by microplate reader. Total GSH levels were determined based on absorbance measurements at 405 nm using a microplate reader and normalized to the total protein content of each sample.

2.13. Animals and treatments

ICR mice (18-22 g, Laboratory Animal Center, Ningxia Medical University, SYXK Ning 2020-0001) were housed under specific pathogen-free (SPF) conditions. All procedures complied with National

Guidelines for the Care and Use of Laboratory Animals (GB/T35892-2018) and were approved by the Institutional Animal Care Committee at Ningxia Medical University (No. 2022-N123). After one-week acclimatization, all mice were randomly assigned as follows: the blank control group (Control), the model group (LPS), the positive drug group (Dexamethasone, DEX), the low-dose GAELNs group at 25 mg/kg, the medium-dose GAELNs group at 50 mg/kg, and the high-dose GAELNs group at 100 mg/kg. The Control and LPS groups were treated with pure water, while the other groups were administered orally with GAELNs or DEX for 7 days. Subsequently, all groups except Control received 5 mg/kg LPS via intratracheal instillation, while Control received saline. After 24 h, mice were euthanized for bronchoalveolar lavage fluid (BALF) and lung tissue collection. BALF was collected by three sequential instillations of 1 mL ice-cold PBS per mouse, yielding ~2 mL total volume for analysis. Major organs (heart, liver, spleen, lungs, kidneys) were excised, saline-rinsed, and processed for histopathology. Daily monitoring included activity, coat condition, food intake, and body weight.

To assess the involvement of the cGAS-STING pathway in GAELN-mediated protection against LPS-induced ALI, mice received DMXAA (5 mg/kg, i.p.), a STING activator, 1 h before LPS challenge. The rest of the processing is the same as above.

2.14. Hematoxylin-Eosin (HE) staining

Lung tissues were fixed in 4% paraformaldehyde, paraffin-embedded, and sectioned at 5 μm thick slices. After dewaxing and rehydration, sections were hematoxylin and eosin (HE) stained for histological evaluation. Images were acquired using an Olympus BX53 microscope (Tokyo, Japan).

2.15. RNA-seq Analysis

Total RNA was isolated from the frozen lung tissues (n = 3 per group) using TRIzol reagent (Invitrogen, USA) according to the manufacturer's instructions. The RNA integrity and concentration were assessed using an Agilent 2100 Bioanalyzer (Agilent Technologies, USA), and only samples with an RNA Integrity Number (RIN) greater than 7.0 were used for subsequent library construction. The sequencing libraries were prepared with the NEBNext® Ultra™ II RNA Library Prep Kit (NEB, USA) and quantified by qPCR. High-throughput sequencing was performed on an Illumina NovaSeq 6000 platform (Novogene Co., Ltd., China) to generate 150 bp paired-end reads. The raw reads were first processed through fastp to remove low-quality sequences and adapters, obtaining clean reads. These high-quality clean reads were then aligned to the reference genome (Mus musculus, GRCm39) using HISAT2. The aligned reads were assembled and the abundance of each transcript was quantified as Fragments Per Kilobase of transcript per Million mapped reads (FPKM) using StringTie. Differential expression analysis between groups was conducted with the DESeq2 R package. Genes with an adjusted $P < 0.05$ and an absolute fold change > 2 were considered statistically significant differentially expressed genes. Functional enrichment analyses, including GO and KEGG pathway analyses, were performed on the differentially expressed genes using the clusterProfiler R package, with a significance threshold of adjusted $P < 0.05$.

2.16. Enzyme-linked immunosorbent assay (ELISA)

The lung tissue samples were homogenized and then centrifuged at 12,000 g at 4°C for 15 min. The protein concentration in the resulting supernatants was determined using a BCA protein assay kit (KeyGEN, China). IL-1β and TNF-α concentrations in lung tissue samples and TNF-α and IL-6 concentrations in BALF were quantified using species-specific ELISA kits following the manufacturers' protocols.

2.17. Real-Time quantitative PCR (RT-qPCR)

Total RNA was extracted from lung tissue samples using an RNA extraction buffer (AXYGEN, China), followed by cDNA synthesis with All-in-One First-Strand cDNA Synthesis SuperMix (One-Step gDNA Removal; TransGen Biotech). RT-qPCR amplification was performed with TipGreen qPCR SuperMix (TransGen Biotech) using the following primers: *IL-1β* (forward: TGAAGTTGACGGACCCCAAAAGAT, reverse: GTTGATGTGCTGCTGCGAGATTTG), *TNF-α* (forward: CAGGTTCTCTTCAAGGGACAAGGC, reverse: TGACGGCAGAGAGGAGGTTGAC), *IL-6* (forward: AGACTTCCATCCAGTTGCCTTCTTG, reverse: TCTGTTGGGAGTGGTATCCTCTGTC), and *GAPDH* (forward: GGTTGTCTCCTGCGACTTCA, reverse: TGGTCCAGGGTTTCTTACTCC). Relative gene expression was calculated via the $2^{-\Delta\Delta Ct}$ method.

2.18. Western blot

Total protein extraction from lung tissues was performed according to the guidelines provided in the whole-cell lysis assay (KeyGEN, China). The protein concentration in the extracts was measured using the BCA protein assay kit (KeyGEN, China). Equal amounts of total protein (50 μg) were separated by 10% SDS-PAGE and transferred onto PVDF membranes. The membranes were blocked with 5% non-fat milk for 1 h and then incubated with primary antibodies targeting IL-1β, IL-6, TNF-α, cGAS, STING, TBK1, p-TBK1, IRF3, and p-IRF3 overnight at 4°C. After washing with TBST, the membranes were incubated with the corresponding secondary antibodies for 2 h. Protein band intensities were quantified using the ImageJ software.

2.19. Immunofluorescence staining

Mouse lung tissues were fixed in 4% paraformaldehyde (PFA) for 24 h at 4°C, paraffin-embedded, and sectioned at 5 μm. Sections were deparaffinized, rehydrated, and subjected to antigen retrieval in pre-heated sodium citrate buffer (10 mM, pH 6.0) at 95°C for 20 min. After cooling and permeabilization with 0.3% Triton X-100 in PBS, non-specific binding was blocked with 5% normal serum/1% BSA in PBS for 1h at room temperature (RT). Sections were then incubated sequentially with anti-cGAS (1:100), anti-STING (1:100), and anti-IRF3 (1:100) primary antibodies, and each applied overnight at 4°C. After PBS washes, sections were sequentially incubated with a fluorophore-conjugated secondary antibodies for 1 h at RT in the dark, including Alexa Fluor 594 (red) for cGAS, Alexa Fluor 488 (green) for STING, and Alexa Fluor 555 (yellow emission) for IRF3, followed by nuclear counterstaining with DAPI (1 μg/mL). Images were captured with a laser-scanning confocal microscopy (Olympus Fluoview FV1000, Japan).

2.20. Toxic effects of GAELNs on mouse organs observed by HE staining

After one week of adaptive feeding, six ICR mice, weighing 18-22 g, were given 100 mg/kg of GAELNs by gavage daily for 7 consecutive days. After resting for 6 h, the liver, heart, spleen, lung and kidney tissues were sampled and fixed with 4% paraformaldehyde, dehydrated with ethanol gradient, treated for transparency with xylene, impregnated with wax, and embedded with paraffin. Then, discontinuous 5 μm-thick sections were sliced, stained with HE, dehydrated, treated for transparency, and sealed properly. The toxic effects were observed under a microscope.

2.21. Statistical analysis

The data are presented as mean ± standard deviation (SD). One-way analysis of variance (ANOVA) with Tukey's post-hoc test was used to analyze the differences between groups using GraphPad Prism 9.3 software (San Diego, USA). P-values less than 0.05 were considered statistically significant.

3. Results

3.1. Identification and characterization of GAELNs

As displayed in Fig. 1A, GAELNs were isolated from fresh garlic using ultracentrifugation and sucrose gradient centrifugation, with precipitation observed at the 30% ~ 45% interface (Fig. 1B). TEM observations revealed that GAELNs exhibited a characteristic spherical or saucer-shaped vesicle morphology (Fig. 1C), with a diameter distribution ranging from 100 to 200 nm. DLS via a nanoparticle analyzer was employed to assess the particle size and Zeta potential of GAELNs. As shown in Fig. 1D, the size analysis indicated an average hydrodynamic diameter of approximately 150 nm for GAELNs, with a particle concentration of approximately 1×10^{10} particles/mL. Zeta potential, a key parameter for evaluating the colloidal stability of nanoparticles, typically reflects stable dispersion when its absolute value ranges between 30 mV and -30 mV. As illustrated in Fig. 1E, the Zeta potential of GAELNs in aqueous solution was measured at -7.8 mV, indicating their relatively stable colloidal dispersion state in the solution.

To elucidate the composition of GAELNs, we firstly conducted LC-MS-based component analysis. As shown in Fig. 1F, fatty acids constituted the largest proportion (27.03%) of GAELNs, subsequently followed by terpenoids (18.71%), shikimates and phenylpropanoids (14.55%), alkaloids (8.11%), polyketides (5.61%), carbohydrates (4.37%), amino acids and peptides (2.70%). Especially organic sulfur compounds (0.42%), such as DATS and DADS, were all detected. These small-molecule metabolites demonstrate significant potential in regulating physiological functions and exerting pharmacological effects, while also playing critical roles in maintaining plant health and enhancing resistance to external stresses.

We further analyzed its lipid composition using non-targeted lipid metabolomics. As illustrated in Fig. 1G, a total of 53 lipid molecules were identified and classified into five major categories, including glycerolipids (GL), glycerophospholipids (GP), sphingolipids (SP), fatty acyls (FA), and sterol lipids (ST). Components exceeding 5% in abundance included glycosyldiacylglycerol (GDG, 17.31%), triacylglycerols (TAGs, 14.7%), betaine diacylglycerol (DGTS, 11.72%), choline glycerophosphate (GPC, 7.26%), ethanolamine glycerophosphate (GPE, 6.45%), diacylglycerol (DAG, 6.33%), ceramide (Cer, 5.65%), and

sphingomyelin phosphate (5.46%). Notably, Cer, a key component facilitating or inducing membrane curvature during ELNs biogenesis and secretion, was prominently identified. GDG may play a role in immune responses by modulating immune system activity. Additionally, GDG was shown to stabilize PDNVs during freeze-thaw cycles and lyophilization, preserving their structural and functional integrity. Collectively, GAELNs are rich in various lipid components, which is consistent with the fact that PDNVs are abundant in phospholipids, providing a critical foundation for further exploration of their biological functions.

Meanwhile, label free quantitative proteomics analysis was performed to characterize the protein composition of GAELNs. As illustrated in Fig. 1H, SDS-PAGE analysis revealed that the molecular weights of proteins in GAELNs were predominantly below 75 kDa, providing crucial insights into their protein profile and functional characteristics. A total of 122 proteins and 665 peptide sequences were identified in GAELNs (Fig. 1I, Table S1, and Table S2). These included key enzymes involved in the biotransformation of secondary metabolites in garlic, such as alliin lyase 1, alliinase, and divinyl ether synthase, as well as potential exosomal marker proteins such as cytosolic proteins (e.g., aquaporins), heat shock protein 70 (HSP70), actin, and tubulin. These proteins are commonly linked to vesicle structure, stress response, and intracellular transport mechanisms.

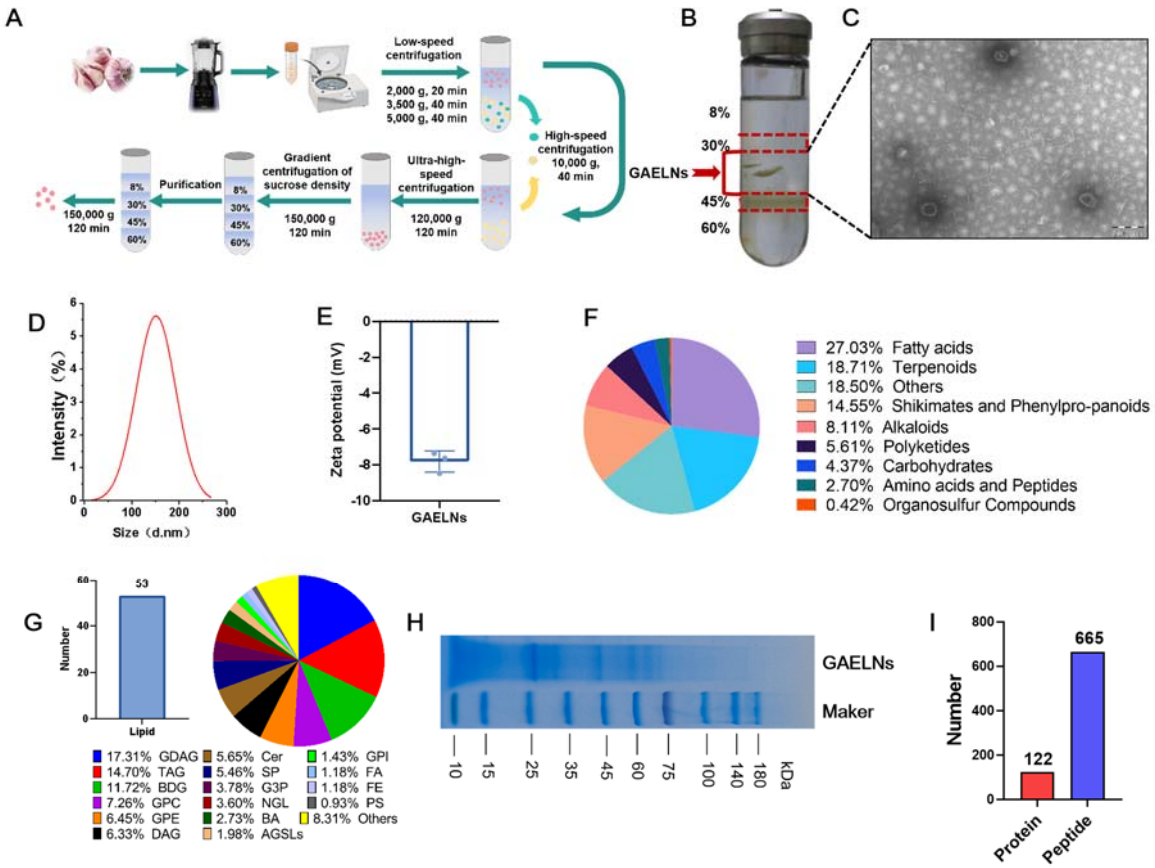

Fig. 1. Preparation, characterization, and composition analysis of GAELNs. (A) Schematic workflow for GAELNs isolation from fresh garlic. (B) GAELNs localized at the 30% ~ 45% sucrose density gradient interface. (C) TEM image revealing GAELNs morphology (scale bar: 200 nm). (D) Size distribution profile determined by DLS. (E) Zeta potential measurement. (F) Analysis of GAELNs-associated small molecules. (G) Quantitative lipidomic analysis showing lipid classes within GAELNs. (H) Coomassie brilliant blue-stained gel of GAELNs proteins. (I) Summary of identified proteins and unique peptide sequences.

Besides, miRNA profiling was performed on GAELNs. Following total RNA extraction, cDNA libraries were constructed and sequenced, yielding raw read data. Analysis of these reads generated unique sequence counts and their corresponding copy numbers. After stringent filtering, 36.85% of the unique sequences were retained as reliable miRNA candidates (Fig. 2A). Subsequent screening for sequences between 18 ~ 25 nucleotides in length (Fig. 2B) identified 254 novel and 224 known miRNAs within GAELNs (Fig. 2C). Notably, the five most abundant miRNAs collectively represented 88.50% of the total miRNA population (Fig. 2D). Subsequently, we further conducted functional enrichment analysis of miRNA target genes in GAELNs. The results of GO analysis are shown in Fig. 2E. The target genes related to miRNAs are associated with various biological processes, cellular components and molecular functions, such as ribonuclease activity, plant-type cell wall, serine-type endopeptidase activity, etc. In KEGG analysis, as shown in Fig. 2F, the signaling pathways of fatty acid biosynthesis, alpha-linolenic acid metabolism, biotin metabolism, and fatty acid degradation were significantly enriched.

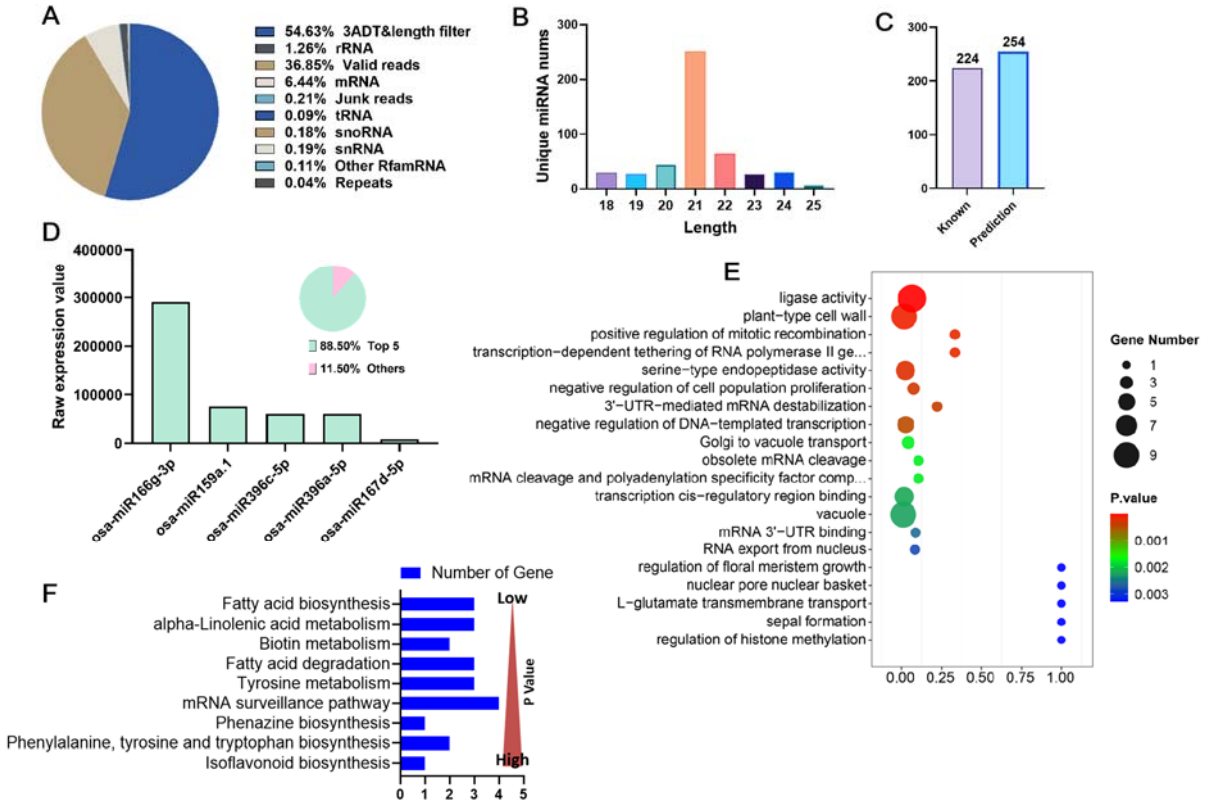

Fig. 2. Identification and functional analysis of miRNAs within GAELNs. (A) Classification of small nucleic acids contained in GAELNs. (B) Length distribution of unique sequences (18 ~ 25 nucleotides) retained after filtering. (C) Classification of identified miRNAs, comprising 254 novel and 224 known species. (D) Relative abundance of the top five most prevalent miRNAs. (E) GO enrichment analysis of predicted miRNA target genes. (F) KEGG pathway enrichment analysis of predicted miRNA target genes.

3.2. GAELNs mitigates LPS-induced RAW264.7 cells inflammatory response

To explore the protective effects of GAELNs on LPS-induced RAW264.7 cell injury at the cellular level, we first evaluated cell viability using the CCK-8 assay. As shown in Fig. 3A, RAW264.7 cell proliferation activity remained unaffected at GAELNs concentrations ≤ 593.75 μg/mL. Based on these findings, non-cytotoxic concentrations of GAELNs were selected for subsequent experiments. Firstly, the

Griess reagent assay was employed to assess the inhibitory effects of GAELNs on LPS-induced inflammation by measuring NO levels in cell culture supernatants. Compared to the Control group, LPS stimulation significantly increased NO release in RAW264.7 cells ($P < 0.001$, Fig. 3B), confirming successful induction of the inflammatory model. GAELNs treatment markedly suppressed LPS-induced NO overproduction ($P < 0.01$ vs. LPS group), with the most pronounced effect observed at 593.75 μg/mL. This concentration was thus selected for further studies. Then, the mRNA expression of TNF-α, IL-1β, and IL-6 were detected by RT-qPCR. The results showed that LPS treatment notably increased the levels of TNF-α, IL-1β, and IL-6 ($P < 0.001$), while the increases in the expression of TNF-α, IL-1β, and IL-6 induced by LPS was reduced after treatment with GAELNs ($P < 0.001$, Fig. 3C-E). In addition, the impact of GAELNs on GSH and ROS levels in LPS-treated RAW264.7 cells were evaluated. LPS exposure significantly reduced GSH ($P < 0.001$) and increased ROS ($P < 0.01$) content compared to the Control group, while GAELNs treatment restored GSH content ($P < 0.01$, Fig. 3F) and effectively inhibited ROS overproduction ($P < 0.05$, Fig. 3G, H). These findings underscore the potential of GAELNs in mitigating oxidative stress and inflammation in LPS-challenged macrophages.

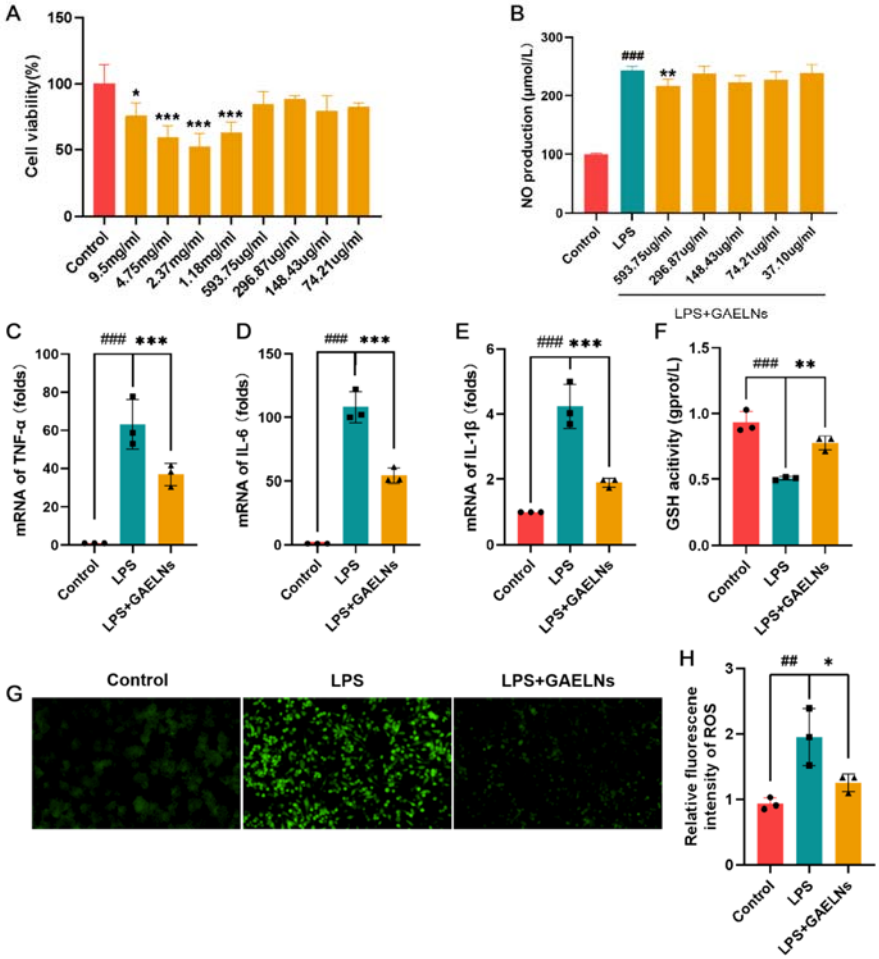

Fig. 3. GAELNs protects against LPS-induced injury in RAW264.7 macrophages. (A) Cell viability assessed by CCK-8 assay. (B) NO production measured by Griess assay in cell supernatants. The mRNA expression of (C) TNF-α, (D) IL-1β, and (E) IL-6 were detected by RT-qPCR. (F) Intracellular GSH levels. (G) Representative images and (H) quantification of intracellular ROS detected by DCFH-DA fluorescence. Data represent mean ± SD (n ≥ 3). Statistical analysis was carried out with one-way ANOVA with Tukey multiple comparisons. n represents the number of biological replicates. $^{\#\#}P < 0.01$, $^{\#\#\#}P < 0.001$ vs. Control group, $^{*}P < 0.05$, $^{**}P < 0.01$, $^{***}P < 0.001$ vs. LPS group.

3.3. GAELNs ameliorates LPS-induced ALI

Pathological observation is the gold standard assessing the degree of lung injury, herein HE staining was used to analyze the pathological changes of mouse lung tissue. As shown in Fig. 4A, B, GAELNs (100, 50, and 25 mg/kg) significantly alleviated LPS-induced ALI in mice. Specifically, the Control group exhibited intact alveolar architecture with no pathological abnormalities. In contrast, LPS-induced ALI mice displayed characteristic pathological alterations, including widened alveolar septa, disrupted alveolar walls, erythrocyte exudation, alveolar collapse, interstitial fibrosis, and substantial infiltration of neutrophils and macrophages. Compared to the LPS group, all GAELNs dose groups and the DEX-positive control markedly mitigated these pathological changes. The GAELNs 100 mg/kg group showed the most significant reduction in inflammatory cell infiltration and tissue damage. We further used the lung injury scoring system to determine the degree of injured lung tissue. As illustrated in Fig. 4C, histopathological scoring confirmed significantly elevated lung injury severity in the LPS group compared to controls ($P < 0.05$). GAELNs administration resulted in a dose-dependent reduction in histological scores ($P < 0.05$ vs. LPS group), validating a dose-responsive protective effect against LPS-induced ALI.

Subsequently, ELISA was used to detect the inflammation in BALF and lung tissue of mice in each group. As displayed in Fig. 4D-G, ELISA analysis revealed markedly elevated levels of IL-6 and TNF-α in BALF and upregulated expression of TNF-α and IL-1β in lung tissues in LPS-treated mice. While GAELNs dose-dependently suppressed the overexpression of these pro-inflammatory mediators, with maximal inhibition observed at 100 mg/kg. Collectively, GAELNs alleviated LPS-induced ALI by reducing histopathological damage, inhibiting inflammatory cell infiltration, and downregulating pro-inflammatory cytokines in a dose-dependent manner. These findings suggest that GAELNs exerts lung protection via modulation of inflammatory cascades.

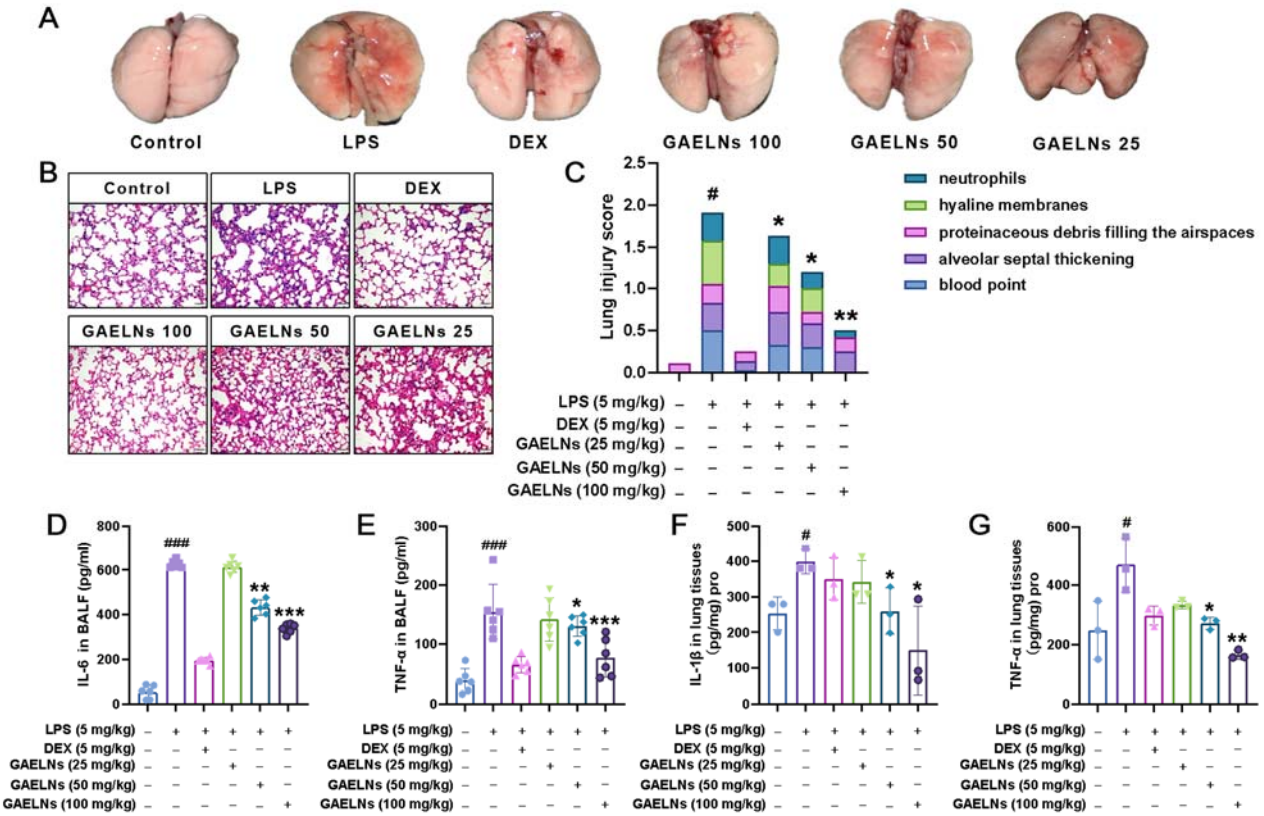

Fig. 4. GAELNs ameliorates LPS-induced ALI in mice. (A) Representative images of the lungs. (B) Representative HE-stained lung tissue sections (scale bar: 200 μm). (C) Quantitative histopathological injury scores. (D-G) Levels of inflammatory cytokines including (D) IL-6 and (E) TNF-α in BALF (n = 6), (F) IL-1β and (G) TNF-α in lung tissue homogenates. Data represent mean ± SD (n = 3). Statistical analysis was carried out with one-way ANOVA with Tukey multiple comparisons. n represents the number of biological replicates. $^{\#}P < 0.05$, $^{\#\#\#}P < 0.001$ vs. Control group, $^{*}P < 0.05$, $^{**}P < 0.01$, $^{***}P < 0.001$ vs. LPS group.

3.4. RNA-seq analysis reveals molecular insights into GAELNs-mediated alleviation of LPS-induced ALI in mice

To investigate the mechanism of GAELNs against ALI, RNA-seq was performed on lung tissues from ALI mice for bioinformatics analysis. As illustrated in Fig. 5A, the heat map results indicated that there were significant differences in the gene expression profiles between the GAELNs treatment group and the LPS group. Subsequently, KEGG pathway enrichment analysis displayed in Fig. 5B revealed that GAELNs influenced multiple inflammatory signaling pathways, including TNF signaling pathway, NF-κB signaling pathway, IL-17 signaling pathway, chemokine signaling pathway, and NOD-like receptor signaling pathway.

To validate the RNA-seq results, RT-qPCR was performed to assess transcriptional changes in TNF-α, IL-6, and IL-1β. As shown in Fig. 5C-E, the LPS group demonstrated significantly elevated mRNA levels of TNF-α ($P < 0.01$), IL-6 ($P < 0.001$), and IL-1β ($P < 0.01$) compared to the Control group. In contrast, GAELNs treatment markedly reduced pulmonary mRNA expression of TNF-α ($P < 0.01$), IL-6 ($P < 0.001$), and IL-1β ($P < 0.05$) relative to the LPS group. The same result was also verified at the protein level, as shown in the Fig. 5F-H. Overall, these results indicate that GAELNs may alleviate ALI in mice primarily through modulation of inflammation and immune response related signaling pathways.

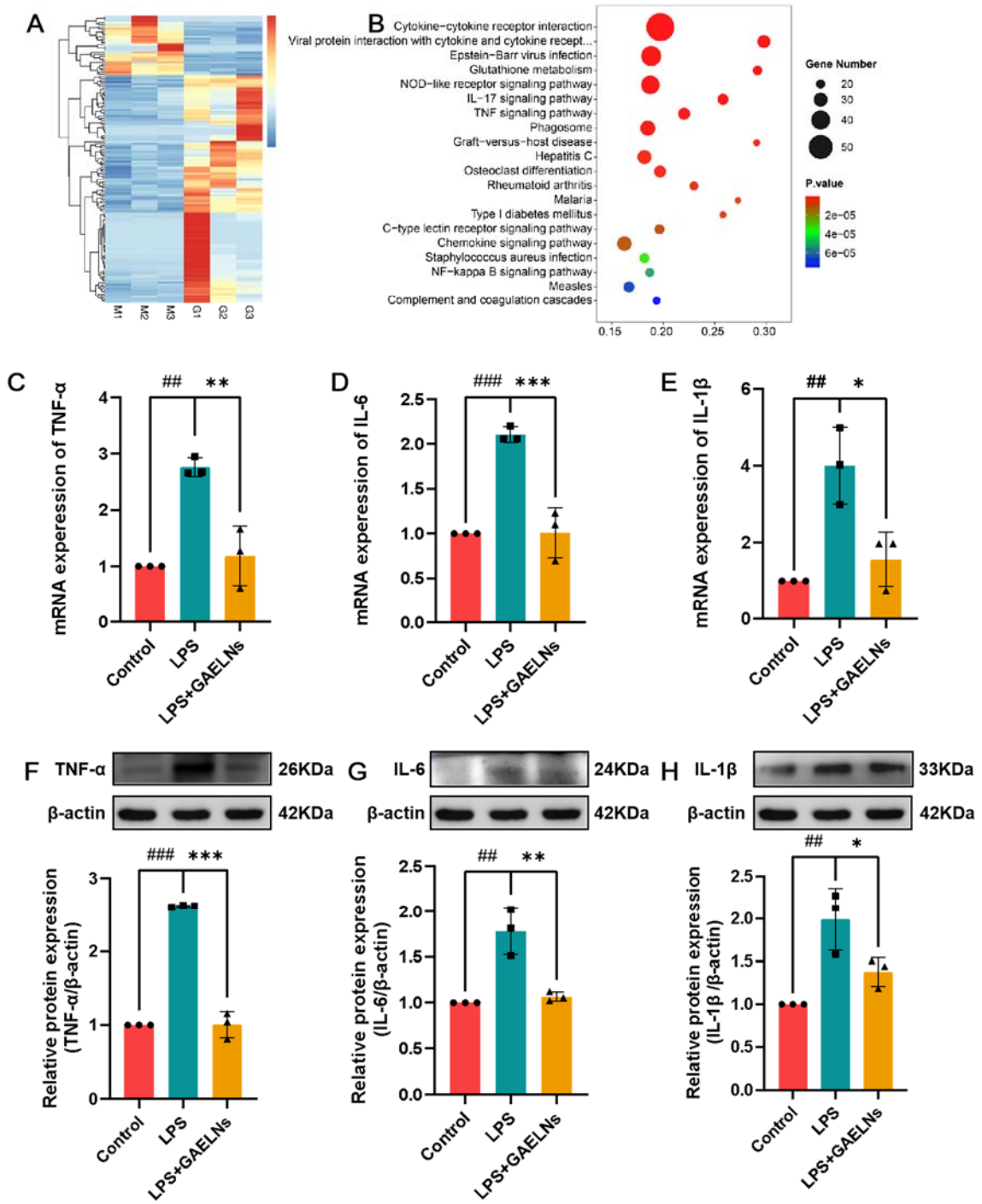

Fig. 5. Transcriptomic analysis and validation of the anti-inflammatory mechanism of GAELNs in LPS-induced ALI. (A) Heatmap demonstrating differential gene expression profiles in lung tissues of LPS-challenged mice treated with or without GAELNs. (B) KEGG pathway enrichment analysis revealing significant modulation of inflammatory signaling pathways by GAELNs. (C-E) Relative mRNA expression levels of (C) TNF-α, (D) IL-6, and (E) IL-1β in lung tissue measured by RT-qPCR. (F-H) Protein expression levels of (F) TNF-α, (G) IL-6, and (H) IL-1β in lung tissue determined by western blot (representative blots shown) with quantitative densitometry. Data represent mean ± SD (n = 3). Statistical analysis was carried out with one-way ANOVA with Tukey multiple comparisons. n represents the number of biological replicates. $^{\#\#}P < 0.01$, $^{\#\#\#}P < 0.001$ vs. Control group, $^{*}P < 0.05$, $^{**}P < 0.01$, $^{***}P < 0.001$ vs. LPS group.

3.5. GAELNs attenuates NF-κB Pathway Activation in LPS-Induced ALI

The NF-κB signaling pathway is a canonical mediator of inflammatory responses. In the present study, Western blot analysis was performed to evaluate the expression of IκBα/NF-κB pathway-related proteins, including p65, p-p65, IκBα, and p-IκBα, in mice lung tissues. As shown in Fig. 6, compared to the Control

group, LPS exposure significantly upregulated pulmonary protein levels of p65 ($P < 0.05$), p-p65 ($P < 0.05$), and p-IκBα. GAELNs treatment markedly reduced the expression of p65 ($P < 0.05$, Fig. 6A), p-p65 ($P < 0.05$, Fig. 6B), and p-IκBα ($P < 0.05$, Fig. 6D) relative to the LPS group. Conversely, GAELNs enhanced IκBα expression ($P < 0.05$, Fig. 6C) compared to the LPS group. These findings suggest that GAELNs might ameliorate LPS-induced pulmonary inflammation in mice by modulating the IκBα/NF-κB signaling pathway.

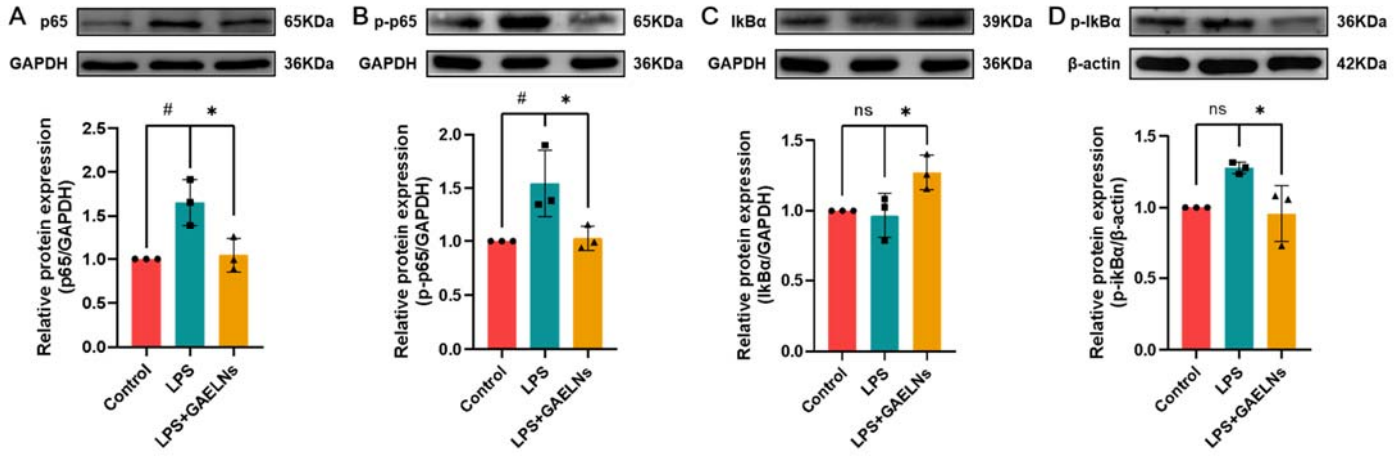

Fig. 6. GAELNs inhibits LPS-induced NF-κB pathway activation in murine lung tissue. Western blot analysis and quantification of key NF-κB signaling components including (A) p65, (B) p-p65, (C) IκBα, and (D) p-IκBα protein expression levels. Representative blots shown above corresponding graphs. Data represent mean ± SD (n = 3). Statistical analysis was carried out with one-way ANOVA with Tukey multiple comparisons. n represents the number of biological replicates. $^{\#}P < 0.05$ vs. Control, $^{*}P < 0.05$ vs. LPS group.

3.6. GAELNs Attenuates cGAS-STING Pathway Activation in LPS-Induced ALI

The cGAS-STING signaling pathway has emerged as a critical inflammatory mediator in tissue injury microenvironments. To assess the modulatory effects of GAELNs on cGAS-STING signaling pathway in ALI mice, Western blot analysis was performed to evaluate pulmonary cGAS and STING protein expression. As shown in Fig. 7, LPS exposure significantly upregulated cGAS ($P < 0.05$) and STING ($P < 0.05$) protein levels compared to the Control group. Conversely, GAELNs treatment markedly reduced both cGAS ($P < 0.05$, Fig. 7A, B) and STING ($P < 0.05$, Fig. 7A, C) expression relative to the LPS group. These results demonstrate that GAELNs suppress LPS-induced cGAS and STING protein expression in ALI mice. TBK1, a direct downstream substrate of STING, undergoes phosphorylation by STING and subsequently regulates IRF3 activation to amplify inflammatory responses. Western blot analysis of STING downstream targets revealed that LPS exposure significantly increased pulmonary expression of p-TBK1 ($P < 0.001$, Fig. 7D, E), TBK1 ($P < 0.01$, Fig. 7D, F), p-IRF3 ($P < 0.05$, Fig. 7D, H), and IRF3 ($P < 0.001$, Fig. 7D, G) compared to the Control group. As expected, GAELNs treatment attenuated these LPS-induced elevations in p-TBK1 ($P < 0.001$, Fig. 7D, E), TBK1 ($P < 0.05$, Fig. 7D, F), p-IRF3 ($P < 0.05$, Fig. 7D, H), and IRF3 ($P < 0.001$, Fig. 7D, G) protein levels. Furthermore, nuclear translocation of IRF3, a hallmark of pathway activation, was analyzed. Results in Fig. 7I, J demonstrate that LPS induce markedly enhanced nuclear IRF3 expression ($P < 0.01$), while GAELNs treatment significantly suppressed this nuclear accumulation ($P <$

0.05). Furthermore, immunofluorescence staining also demonstrated the same expression trend of the above-mentioned proteins (Fig. 7K). Collectively, these findings suggest that GAELNs confer protection against LPS-induced ALI by modulating the cGAS-STING signaling axis, thereby inhibiting TBK1-IRF3 phosphorylation and nuclear translocation.

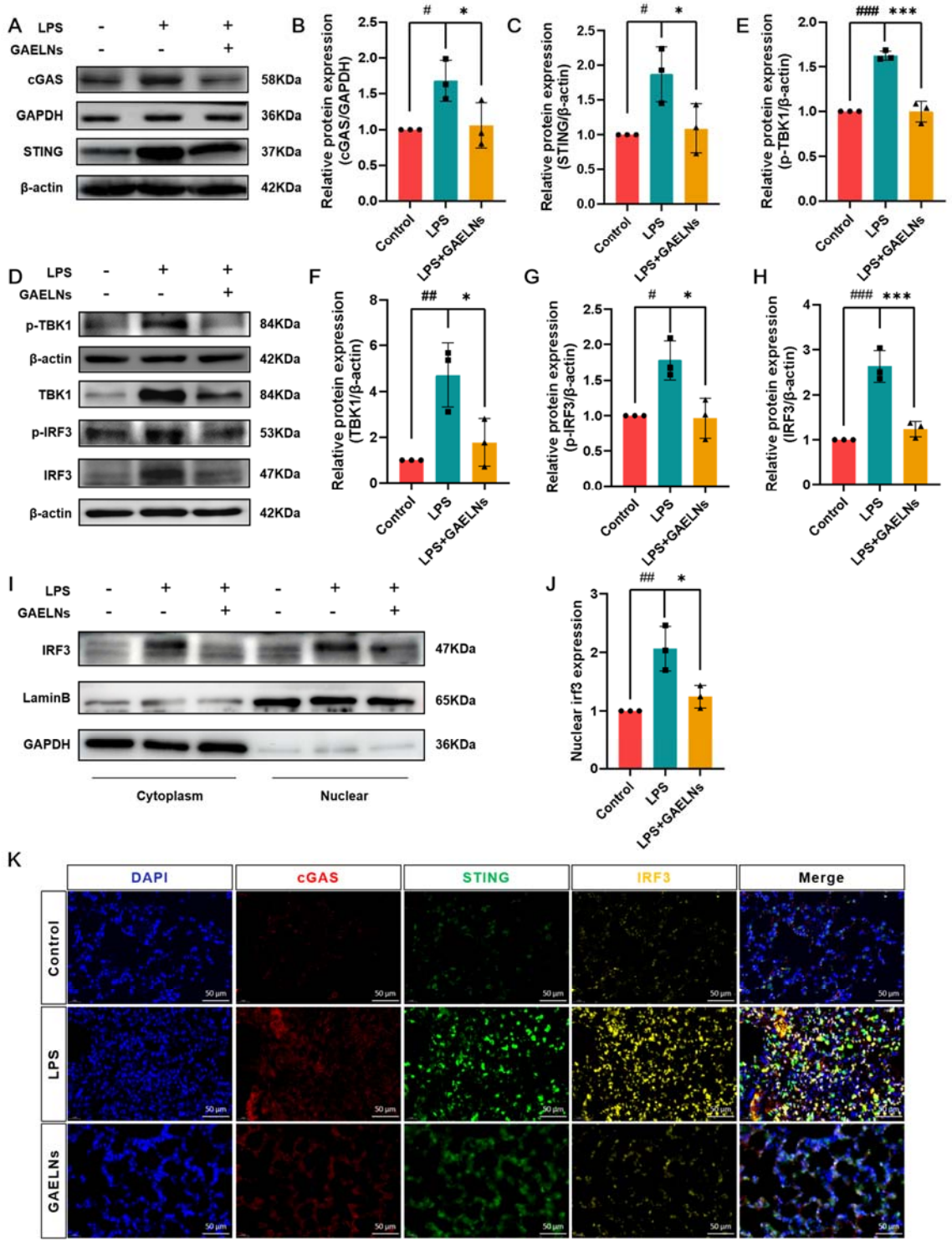

Fig. 7. GAELNs attenuates LPS-induced activation of the cGAS-STING-TBK1-IRF3 signaling axis in murine lung tissue. (A) Representative Western blots and quantitative analysis of (B) cGAS and (C) STING protein expression. (D) Representative Western blots and quantitative analysis of key downstream mediators including (E) p-TBK1, (F) TBK1, (G) IRF3, and (H) p-IRF3. (I) Representative Western blots and (J) quantification of nuclear IRF3 expression. (K) Representative immunofluorescence images confirming protein expression trends. Data represent mean ± SD (n = 3). Statistical analysis was carried out with one-way ANOVA with Tukey multiple comparisons. n represents the number of biological replicates. $^{\#}P < 0.05$, $^{\#\#}P < 0.01$, $^{\#\#\#}P < 0.001$ vs. Control group, $^{*}P < 0.05$, $^{***}P < 0.001$ vs. LPS group.

3.7. GAELNs abrogates the activation of the cGAS-STING pathway induced by the STING agonist DMXAA in LPS-treated mice

To determine whether GAELNs exert their protective effects against LPS-induced ALI via modulation of the cGAS-STING pathway, mice were pretreated with DMXAA (a STING activator) prior to LPS challenge. Results demonstrated that GAELNs significantly attenuated LPS-induced histopathological damage (Fig. 8A-C). Meanwhile, GAELNs abrogates the activation of the cGAS-STING pathway induced by the STING agonist DMXAA in LPS-treated mice, as evidenced by both the histopathological alterations and downregulation of cGAS and STING (Fig. 8D). These findings indicate that the protective effect of GAELNs in LPS-induced ALI is mediated by inhibition of the cGAS-STING signaling pathway.

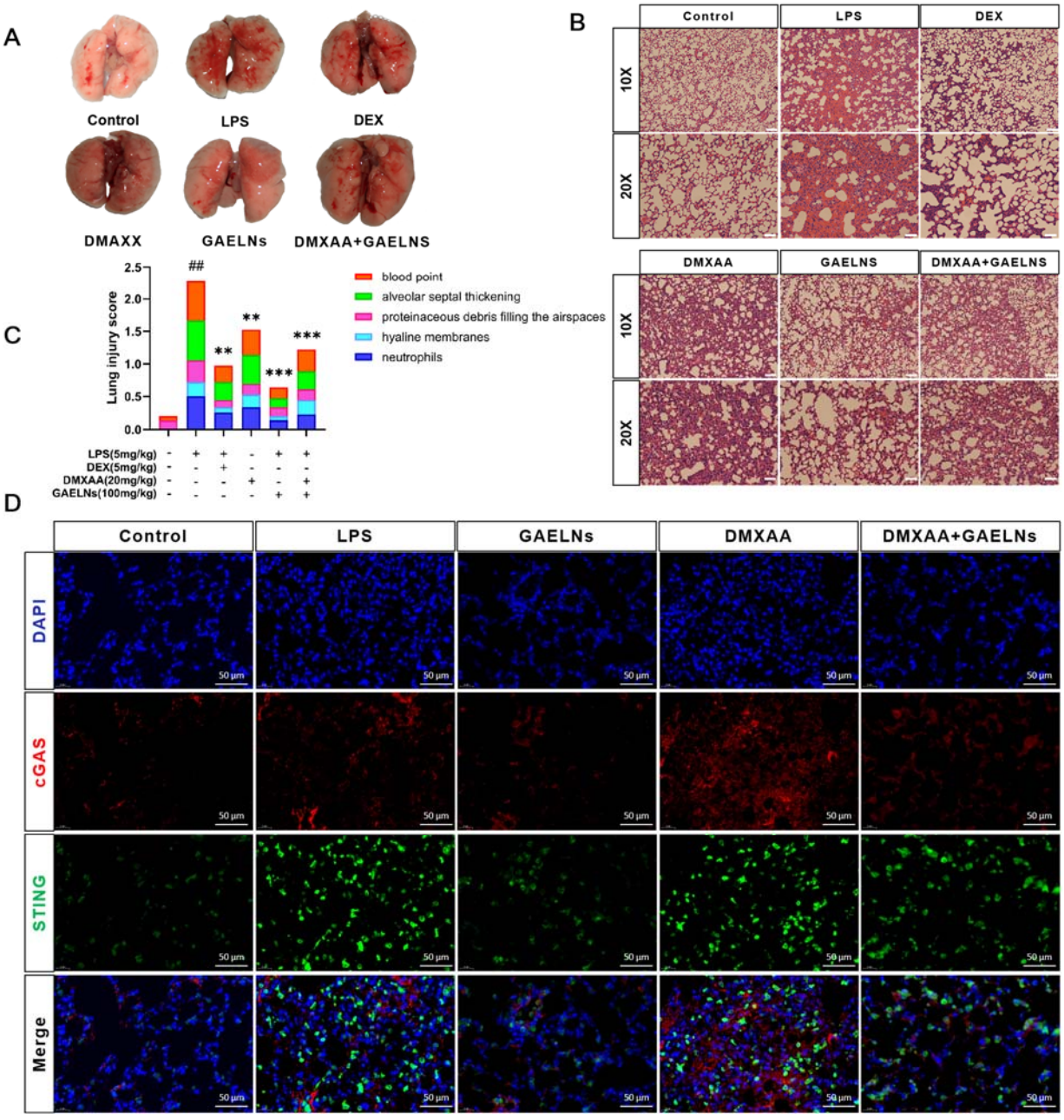

Fig. 8. GAELNs protects against LPS-induced ALI by inhibiting the cGAS-STING pathway. (A) Representative images of the lungs. (B) Representative HE-stained lung tissue sections (scale bar: 200 μm). (C) Quantitative histopathological injury scores. (D) Representative immunofluorescence images of cGAS and STING. Statistical analysis was carried out with one-way ANOVA with Tukey multiple comparisons. n represents the number of biological replicates. $^{\#\#}P < 0.01$ vs. Control group, $^{**}P < 0.01$, $^{***}P < 0.001$ vs. LPS group.

3.8. Favorable acute safety profile of GAELNs demonstrated by organ histopathology

To evaluate the potential acute toxicity of GAELNs, mice were subjected to a daily oral gavage of GAELNs 100 mg/kg for seven consecutive days. Histopathological examination of major visceral organs, including the heart, liver, spleen, lung, and kidney, revealed no significant structural abnormalities or lesions (Fig. S1). This absence of observable adverse effects across these critical organ systems indicates that GAELNs were well-tolerated at the administered dosage. Collectively, these findings demonstrate a favorable preliminary safety profile, suggesting low or negligible systemic toxicity for GAELNs *in vivo*.

4. Discussion

ALI is a life-threatening inflammatory syndrome. Despite medical advancements, mortality exceeds 40% due to the absence of therapies and limitations of current treatments relying on antibiotics and glucocorticoids, which frequently induce adverse effects. Emerging evidence highlights dysregulated systemic inflammation as the core pathogenic mechanism, necessitating interventions targeting both primary triggers and subsequent inflammatory cascades. This therapeutic gap has intensified research into plant-derived anti-inflammatory compounds as novel alternatives, given the potential to modulate inflammatory pathways with improved safety profiles.

PDNVs have emerged as promising therapeutic agents due to the advantages of biocompatibility, cost-effectiveness, environmental sustainability, and scalability for mass production [38]. Garlic demonstrates potent anti-inflammatory effects through NF-κB pathway inhibition, with documented efficacy against pulmonary inflammation. Recent studies highlight GAELNs as multi-targeted therapeutics, alleviating metabolic and inflammatory disorders via TLR4/MyD88/NF-κB and CCR2/CCR5 signaling in conditions ranging from colitis to liver injury [32, 34]. Given this evidence, GAELNs are hypothesized to mitigate ALI through anti-inflammatory mechanisms. To address this issue, this study successfully isolated and purified GAELNs through a combination of ultracentrifugation and sucrose density gradient centrifugation, followed by characterization, compositional analysis, and further investigation of anti-inflammatory effects in LPS-induced RAW264.7 cell and mouse models. The observed therapeutic efficacy may be associated with regulation of the cGAS-STING signaling pathway.

Firstly, the extraction and purification of GAELNs constitute the critical phase of this investigation. In the field of PDNVs isolation, the integration of ultracentrifugation with sucrose density gradient centrifugation represents a widely validated purification strategy [38]. This methodology achieves enhanced vesicle purity through sequential processing, including primary enrichment via ultracentrifugation followed by gradient-based purification. Owing to the demonstrated separation efficacy and reproducibility, this combined protocol has been established as the standardized approach for PDNVs preparation. Employing this optimized workflow, our study successfully isolated GAELNs exhibiting characteristic features of exosome-like particles, including lipid bilayer-enclosed vesicles with a mean diameter of approximately 150 nm and circular or saucer-shaped morphology, consistent with previously documented phytosomal structures [39]. The zeta potential of these vesicles was measured at -7.8 mV, also consistent with previously reports [31].

Zeta potential analysis confirmed the stability of GAELNs, as values within the ± 30 mV range indicate favorable dispersion characteristics [40]. These findings confirm the favorable stability of the GAELNs isolated in this study.

However, the characterization and classification of plant-derived exosomes remain challenging due to the incomplete identification of definitive biomarkers, necessitating the development of robust markers and validation methodologies. To address this, we comprehensively profiled the molecular composition of GAELNs through multi-omics analyses, including untargeted metabolomics, lipidomics, proteomics, and microRNA sequencing. These investigations revealed diverse constituents within GAELNs, encompassing lipid species, protein classes, miRNAs, and secondary metabolites.

Specifically, lipidomic profiling identified over fifty lipid species in GAELNs, including GL, GP, SP, FA, and ST. Exosomal lipid bilayers safeguard encapsulated RNAs and proteins from degradation while maintaining membrane fluidity and elasticity essential for biogenesis and functionality [41]. Notably, lipids may regulate plant immune responses via interactions with cell-surface receptors [42]. For instance, lipids may participate in pathogen recognition and defensive responses against specific microbial threats. Beyond structural stabilization, lipids play pivotal roles in intercellular communication, metabolic regulation, and immune modulation. Cer lipid, a key component facilitating or inducing membrane curvature during EVs biogenesis and secretion through regulatory mechanisms that influence intercellular communication and molecular exchange, was prominently identified in GAELNs [43]. GDG in GAELNs may play a role in immune responses by modulating immune system activity. Additionally, GDG was shown to stabilize plant-derived exosomal vesicles during freeze-thaw cycles and lyophilization, preserving their structural and functional integrity. Collectively, GAELNs are rich in various lipid components, which is consistent with the fact that plant exosomes are abundant in phospholipids, providing a critical foundation for further exploration of their biological functions.

Furthermore, GAELNs were enriched with diverse miRNAs, such as osa-miR166g-3p, osa-miR159a.1, and osa-miR396c-5p, which exhibit functional versatility due to their origins from distinct plant tissues and developmental stages. A hallmark of these miRNAs lies in their capacity to mediate targeted gene regulation, thereby conferring therapeutic potential [44]. Notable examples include honeysuckle derived miR2911 demonstrating antiviral efficacy against influenza by reducing mouse morbidity [45], and *Salvia miltiorrhiza* derived Sal-miR-58 attenuating vascular inflammation through autophagy induction in smooth muscle cells [46]. Ginseng nanovesicles promote wound healing via miRNA transfer to mesenchymal stem cells [47], while bitter melon miR5266 encapsulated in PDNVs exerts neuroprotective effects through blood-brain barrier penetration and MMP9 inhibition [48]. Ginger derived aly-miR396a-5p could abolish lung inflammation [19]. *Carthamus tinctorius* L. derived miR166a-3p mitigates vascular inflammation by targeting endothelial CXCL12 [49], and miR166a-3p was also high expressed with top 7 miRNAs in GAELNs purified from our present study, which might be one of the key material bases for GAELNs to exert their anti-inflammatory effects. Collectively, these findings validate plant miRNAs as bioactive components with translational

medical potential. Of particular note, peu-miR2916-p3-enriched garlic exosomes demonstrate therapeutic efficacy in ameliorating murine colitis through gut microbiota remodeling, further substantiating the healthy-promoting potential of garlic-derived miRNAs [33]. Our present study revealed the enrichment of osa-miR166g-3p in GAELNs. Therefore, subsequent investigations is necessary to evaluate the therapeutic capacity of osa-miR166g-3p or other top high expressed miRNAs in GAELNs against ALI.

Proteomic analysis identified a broad spectrum of proteins associated with critical biological processes, encompassing key enzymes involved in garlic-specific secondary metabolite biotransformation such as alliin lyase 1, alliinase, and divinyl ether synthase, as well as canonical exosomal markers including cytoskeletal proteins actin and tubulin, HSP70, and membrane transport regulators such as aquaporins. These proteins are functionally implicated in vesicle structural integrity, stress adaptation, and intracellular trafficking mechanisms.

Following the elucidation of the chemical composition of GAELNs, we further evaluated the anti-inflammatory efficacy through *in vitro* and *in vivo* experiments. In the LPS-induced RAW264.7 macrophage polarization model, GAELNs demonstrated significant anti-inflammatory activity. Subsequently, the therapeutic efficacy of GAELNs against ALI was investigated using an LPS-induced mouse model. To establish the ALI model, intratracheal instillation of LPS was selected rather than intraperitoneal injection to localize inflammation to the lungs, as systemic inflammation induced by intraperitoneal LPS. Dose optimization revealed that LPS 5 mg/kg effectively induced ALI without excessive severity (Fig. S2), whereas LPS 10 mg/kg caused severe lung injury unsuitable for therapeutic evaluation. Dose-response screening revealed that GAELNs exhibited dose-dependent alleviation of ALI at 25 ~ 100 mg/kg, with 100 mg/kg showing comparable efficacy to DEX, while doses ≤ 10 mg/kg were ineffective (Fig. S3). Therefore, we finally selected GAELNs 25 mg/kg, 50 mg/kg, and 100 mg/kg for activity evaluation experiments. Histopathological analysis and cytokine profiling in lung tissues and BALF confirmed the potent mitigation of GAELNs on LPS-induced lung inflammation. These findings align with previous reports on the broad anti-inflammatory properties of GAELNs in other disease models. It should be noted that in this study, GAELNs was administered by gavage. As a type of PDNVs, GAELNs possess a lipid bilayer structure rich in sphingolipids and phospholipids, which provides inherent stability and protects their contents from degradation in the harsh gastrointestinal environment [50, 51]. Upon oral administration, GAELNs are absorbed through multiple interconnected pathways. They can be taken up by intestinal epithelial cells or immune cells such as macrophages. Following cellular internalization, the bioactive cargo is released either intracellularly or into the mucus layer. These liberated components may then traverse the intestinal barrier via paracellular transport through tight junctions or by entering capillaries, ultimately reaching the systemic circulation [51]. This absorption and distribution mechanism facilitates the delivery of GAELNs-derived components to distant organs, thereby explaining the therapeutic effects observed in this study.

In order to clarify the mechanism of GAELNs in alleviating ALI, we used transcriptome sequencing to detect the gene expression profile of lung tissues in each group. Based on GO enrichment analysis, we

identified that GAELNs regulate biological processes including inflammatory response, immune system response, viral defense response, and apoptotic process, while also influencing chemokine activity and antioxidant activity. KEGG pathway enrichment analysis revealed the involvement of GAELNs in multiple inflammatory signaling pathways, particularly the TNF, NF-κB, IL-17, chemokine, and NOD-like receptor signaling pathways. To validate these findings, we conducted molecular biological experiments. First, western blot analysis was performed to investigate the effect of GAELNs on the NF-κB signaling pathway. NF-κB activation occurs through phosphorylation and degradation of IκBα bound to NF-κB, leading to nuclear translocation of NF-κB and subsequent promotion of inflammatory factor expression. IL-6, TNF-α, and IL-1β are key early inflammatory mediators in inflammatory lung disease [52]. Our results demonstrated that compared with the LPS group, GAELNs administration significantly reduced the expression of p65 and p-p65 proteins in the IκBα/NF-κB pathway while promoting IκBα protein expression in mouse lung tissues. Furthermore, GAELNs effectively suppressed LPS-induced elevation of IL-6, TNF-α, and IL-1β protein levels. Subsequently, we detected the components in cGAS-STING signaling pathway. The cGAS-STING signaling pathway serves as a crucial intracellular innate immune surveillance system, primarily responsible for detecting cytoplasmic abnormal DNA and initiating immune responses. Pathway activation begins with cGAS recognition and binding of double-stranded DNA. Then cGAS catalyzes the production of the second messenger cGAMP, which activates the endoplasmic reticulum-localized STING. Activated STING recruits and phosphorylates TBK1, facilitating IRF3 dimerization and nuclear translocation, thereby initiating transcription of type I interferons (IFN-α/β) and related cytokines to trigger antiviral immune responses [53]. In our present LPS-induced ALI model, significant alterations were observed in key components of the cGAS-STING pathway. Specifically, Compared with the control group, experimental mice exhibited markedly increased cGAS protein expression and corresponding elevation of downstream STING expression in lung tissues. Phosphorylation levels of TBK1 and IRF3 were significantly upregulated. These molecular changes indicate specific activation of the cGAS-STING pathway during ALI, suggesting its involvement in pulmonary inflammation regulation. Notably, GAELNs administration effectively downregulated protein expression in the cGAS-STING pathway. Our findings demonstrate that GAELNs exert regulatory effects on the cGAS-STING signaling pathway by suppressing protein expression levels, consistent with previous reports that GAELNs inhibits cGAS and STING-mediated inflammation in microglia [36]. Interestingly, GAELNs abrogates the activation of the cGAS-STING pathway induced by the STING agonist DMXAA in LPS-treated mice, indicating that the protective effect of GAELNs in LPS-induced ALI is mediated by inhibition of the cGAS-STING signaling pathway. While our present study definitively shows that GAELNs inhibit the cGAS-STING pathway activation, the exact molecular components within GAELNs responsible for this effect are likely diverse and may act synergistically. Our multi-omics profiling of GAELNs provides clues for several non-mutually exclusive hypotheses. The rich and unique lipid composition of GAELNs, particularly the presence of ceramides and glycosyldiacylglycerols, may directly influence the membrane properties of recipient immune cells, potentially modulating the assembly or localization of cGAS-STING

signaling complexes. Moreover, the enriched miRNAs within GAELNs, such as miR166a-3p and peu-miR2916-p3, are predicted to target genes involved in inflammatory signaling. It is plausible that these plant-derived miRNAs are delivered to murine macrophages and mediate cross-kingdom gene regulation, potentially silencing key components of the cGAS-STING pathway itself or its downstream inflammatory effectors. Future studies are necessary to specifically evaluate the therapeutic potential of osa-miR166g-3p and other highly expressed miRNAs in GAELNs inhibited the cGAS-STING pathway.

5. Conclusion

In conclusion, this study demonstrates that GAELNs effectively mitigates LPS-induced ALI. GAELNs administration significantly attenuated pulmonary histopathological damage, suppressed pro-inflammatory cytokine production *in vivo*, and reduced harmful cytokine secretion *in vitro*. Mechanistically, GAELNs conferred protection by potently inhibiting the cGAS-STING signaling axis and its downstream effectors, specifically suppressing the phosphorylation of TBK1, IRF3, IκBα, and p65. Crucially, GAELNs abrogates the activation of the cGAS-STING pathway induced by the STING agonist DMXAA in LPS-treated mice. The possible mechanism is shown in Fig. 9. Collectively, these findings identify GAELNs as a novel plant-derived nanotherapeutic that alleviates ALI primarily through inhibition of the cGAS-STING-IRF3/NF-κB inflammatory cascade, highlighting its significant potential as a candidate agent for ALI treatment.

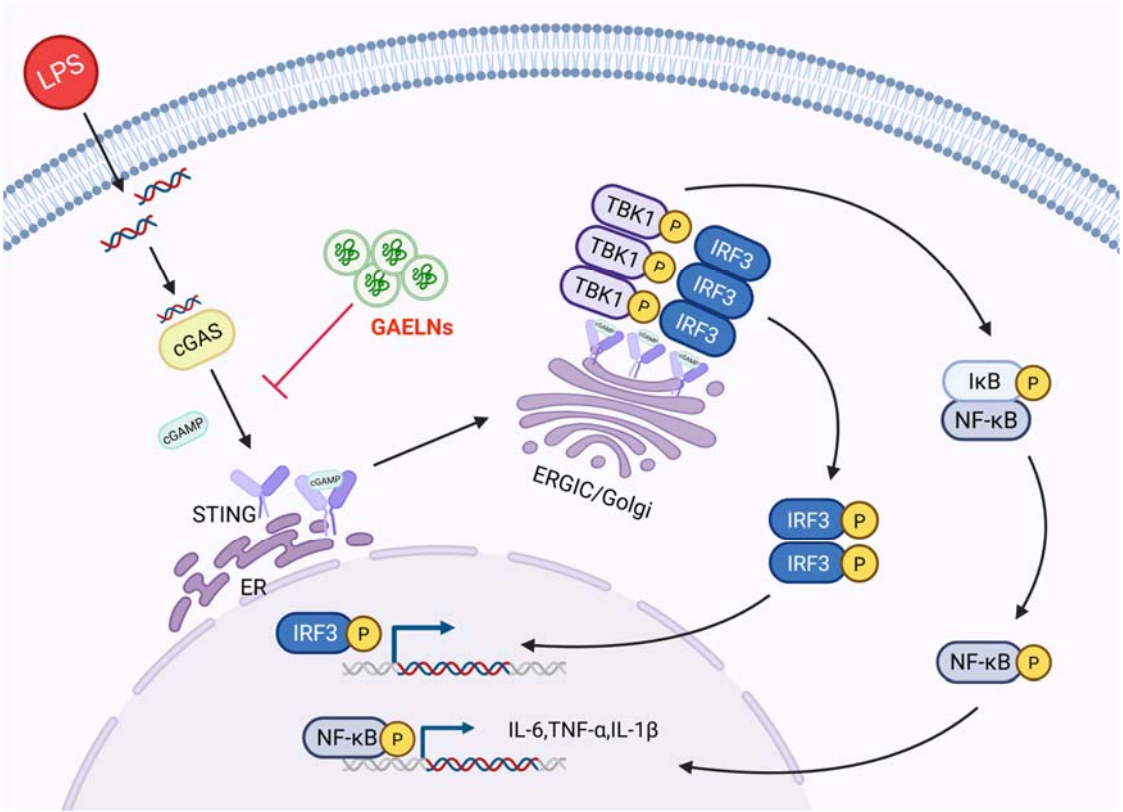

Fig. 9. Proposed mechanism of GAELNs in mitigating LPS-induced ALI. GAELNs exerts protective effects against ALI by potently inhibiting the cGAS-STING signaling axis. This inhibition suppresses the phosphorylation of downstream effectors TBK1 and IRF3, as well as components of the NF-κB pathway, thereby attenuating pro-inflammatory cytokine production. Overall, GAELNs as a novel plant-derived nanotherapeutic that alleviates ALI primarily through inhibition of the cGAS-STING-IRF3/NF-κB inflammatory cascade.

Declaration of Competing Interest

The authors declare no conflict of interest.

Acknowledgments

This work was funded by grants from the National Natural Science Foundation of China (82404632 and 82560715), Key Research and Development Program of Ningxia (2024BEG02012), Natural Science Foundation of Ningxia Province (2023AAC05031), Natural Science Foundation of Hebei Province (H2022423323 and H2019423126), and Research Foundation of Hebei Province Education Department (QN2021107).

References

1. Li Z, Bu Y, Wang C, Yu Y, Han L, Liu C, Chen G, Li C, Zhang Y, Cao H, et al. Extracellular vesicle-packaged GBP2 from macrophages aggravates sepsis-induced acute lung injury by promoting ferroptosis in pulmonary vascular endothelial cells. Redox Biol. 2025;82:103614.
2. Long Matthew E, Mallampalli Rama K, Horowitz Jeffrey C. Pathogenesis of pneumonia and acute lung injury. Clin Sci. 2022;136(10):747-69.
3. Liu C, Xiao K, Xie L. Advances in the use of exosomes for the treatment of ALI/ARDS. Front Immunol. 2022;13:971189.
4. Schouten LRA, Veltkamp F, Bos AP, van Woensel JBM, Serpa Neto A, Schultz MJ, Wösten–van Asperen RM. Incidence and Mortality of Acute Respiratory Distress Syndrome in Children. Crit Care Med. 2016;44(4):819-29.
5. Bellani G, Laffey JG, Pham T, Fan E, Brochard L, Esteban A, Gattinoni L, van Haren F, Larsson A, McAuley DF, et al. Epidemiology, Patterns of Care, and Mortality for Patients With Acute Respiratory Distress Syndrome in Intensive Care Units in 50 Countries. JAMA. 2016;315(8):788.
6. Salazar-Puerta AI, Rincon-Benavides MA, Cuellar-Gaviria TZ, Aldana J, Vasquez Martinez G, Ortega-Pineda L, Das D, Dodd D, Spencer CA, Deng B, et al. Engineered Extracellular Vesicles Derived from Dermal Fibroblasts Attenuate Inflammation in a Murine Model of Acute Lung Injury. Adv Mater. 2023;35(28):e2210579
7. Sun X, Guo C, Huang C, Lv N, Chen H, Huang H, Zhao Y, Sun S, Zhao D, Tian J, et al. GSTP alleviates acute lung injury by S-glutathionylation of KEAP1 and subsequent activation of NRF2 pathway. Redox Biol. 2024;71:103116.
8. Colombo M, Raposo G, Théry C. Biogenesis, Secretion, and Intercellular Interactions of Exosomes and Other Extracellular Vesicles. Annu Rev Cell Dev Biol. 2014;30(1):255-89.
9. Tkach M, Théry C. Communication by Extracellular Vesicles: Where We Are and Where We Need to Go. Cell. 2016;164(6):1226-32.
10. El Andaloussi S, Mäger I, Breakefield XO, Wood MJA. Extracellular vesicles: biology and emerging therapeutic opportunities. Nat Rev Drug Discov. 2013;12(5):347-57.
11. Jung KO, Jo H, Yu JH, Gambhir SS, Pratx G. Development and MPI tracking of novel hypoxia-targeted theranostic exosomes. Biomaterials. 2018;177:139-48.
12. Li W, Liu Y, Zhang P, Tang Y, Zhou M, Jiang W, Zhang X, Wu G, Zhou Y. Tissue-Engineered Bone Immobilized with Human Adipose Stem Cells-Derived Exosomes Promotes Bone Regeneration. ACS Appl. Mater. Interfaces. 2018;10(6):5240-54.
13. Zhang M, Viennois E, Prasad M, Zhang Y, Wang L, Zhang Z, Han MK, Xiao B, Xu C, Srinivasan S, et al. Edible ginger-derived nanoparticles: A novel therapeutic approach for the prevention and treatment of inflammatory bowel disease and colitis-associated cancer. Biomaterials. 2016;101:321-40.
14. Dad HA, Gu TW, Zhu AQ, Huang LQ, Peng LH. Plant Exosome-like Nanovesicles: Emerging Therapeutics and Drug Delivery Nanoplatforms. Mol Ther. 2021;29(1):13-31.
15. Rutter BD, Innes RW. Extracellular Vesicles Isolated from the Leaf Apoplast Carry Stress-Response Proteins. Plant Physiol. 2017;173(1):728-41.

16. Cai Q, Qiao L, Wang M, et al. Plants send small RNAs in extracellular vesicles to fungal pathogen to silence virulence genes. Science. 2018;360(6393):1126-29.
17. Fu J, Liu Z, Feng Z, Huang J, Shi J, Wang K, Jiang X, Yang J, Ning Y, Lu F, et al. Platycodon grandiflorum exosome-like nanoparticles: the material basis of fresh platycodon grandiflorum optimality and its mechanism in regulating acute lung injury. J Nanobiotechnol. 2025;23(1):270.
18. Ye L, Gao Y, Mok SWF, Liao W, Wang Y, Chen C, Yang L, Zhang J, Shi L. Modulation of alveolar macrophage and mitochondrial fitness by medicinal plant-derived nanovesicles to mitigate acute lung injury and viral pneumonia. J Nanobiotechnol. 2024;22(1):190.
19. Teng Y, Xu F, Zhang X, Mu J, Sayed M, Hu X, Lei C, Sriwastva M, Kumar A, Sundaram K, et al. Plant-derived exosomal microRNAs inhibit lung inflammation induced by exosomes SARS-CoV-2 Nsp12. Mol Ther. 2021;29(8):2424-40.
20. De Greef D, Barton EM, Sandberg EN, Croley CR, Pumarol J, Wong TL, Das N, Bishayee A. Anticancer potential of garlic and its bioactive constituents: A systematic and comprehensive review. Semin Cancer Biol. 2021;73:219-64.
21. Rose P, Moore PK, Zhu YZ. Garlic and Gaseous Mediators. Trends Pharmacol Sci. 2018;39(7):624-34.
22. Zhang L, Qu Z, Song A, Yang J, Yu J, Zhang W, Zhuang C. Garlic oil blocks tobacco carcinogen 4-(methylnitrosamino)-1-(3-pyridyl)-1-butanone (NNK)-induced lung tumorigenesis by inducing phase II drug-metabolizing enzymes. Food Chem Toxicol. 2021;157:112581.
23. Tian J, Zhao W, Wu Y, et al. Diallyl Disulfide Blocks Cigarette Carcinogen 4-(Methylnitrosamino)-1-(3-pyridyl)-1-butanone-Induced Lung Tumorigenesis via Activation of the Nrf2 Antioxidant System and Suppression of NF-κB Inflammatory Response J Agric Food Chem. 2023;71(46):17763-74.
24. Qu Z, Tian J, Sun J, Shi Y, Yu J, Zhang W, Zhuang C. Diallyl trisulfide inhibits 4-(methylnitrosamino)-1-(3-pyridyl)-1-butanone-induced lung cancer via modulating gut microbiota and the PPARγ/NF-κB pathway. Food Funct. 2024;15(1):158-71.
25. Abdel-Daim MM, Abushouk AI, Bungau SG, Bin-Jumah M, El-Kott AF, Shati AA, Aleya L, Alkahtani S. Protective effects of thymoquinone and diallyl sulphide against malathion-induced toxicity in rats. Environ Sci Pollut Res Int. 2020;27(10):10228-235.
26. Elmazoglu Z, Aydın Bek Z, Sarıbas SG, Özoğul C, Goker B, Bitik B, Aktekin CN, Karasu C. S-allylcysteine inhibits chondrocyte inflammation to reduce human osteoarthritis via targeting RAGE, TLR4, JNK, and Nrf2 signaling: comparison with colchicine. Biochem Cell Biol. 2021;99(5):645-54.
27. Nie Y, Yu K, Li B, Hu Y, Zhang H, Xin R, Xiong Y, Zhao P, Chai G. S-allyl-l-cysteine attenuates bleomycin-induced pulmonary fibrosis and inflammation via AKT/NF-kappaB signaling pathway in mice. J Pharmacol Sci. 2019;139(4):377-84.
28. Shin NR, Kwon HJ, Ko JW, Kim JS, Lee IC, Kim JC, Kim SH, Shin IS. S-Allyl cysteine reduces eosinophilic airway inflammation and mucus overproduction on ovalbumin-induced allergic asthma model. Int Immunopharmacol. 2019;68:124-30.
29. Wang YL, Guo XY, He W, Chen RJ, Zhuang R. Effects of alliin on LPS-induced acute lung injury by activating PPARgamma. Microb Pathog. 2017;110:375-79.
30. Sundaram K, Mu J, Kumar A, Behera J, Lei C, Sriwastva MK, Xu F, Dryden GW, Zhang L, Chen S, et al. Garlic exosome-like nanoparticles reverse high-fat diet induced obesity via the gut/brain axis. Theranostics. 2022;12(3):1220-46.
31. Bian Y, Li W, Jiang X, Yin F, Yin L, Zhang Y, Guo H, Liu J. Garlic-derived exosomes carrying miR-396e shapes macrophage metabolic reprograming to mitigate the inflammatory response in obese adipose tissue. J Nutr Biochem. 2023;113:109249.
32. Zhu Z, Liao L, Gao M, Liu Q. Garlic-derived exosome-like nanovesicles alleviate dextran sulphate sodium-induced mouse colitis via the TLR4/MyD88/NF-κB pathway and gut microbiota modulation. Food Funct. 2023;14(16):7520-34.
33. Wang X, Liu Y, Dong X, Duan T, Wang C, Wang L, Yang X, Tian H, Li T. peu-MIR2916-p3-enriched garlic exosomes ameliorate murine colitis by reshaping gut microbiota, especially by boosting the anti-colitic Bacteroides thetaiotaomicron. Pharmacol Res. 2024;200:107071.

34. Zhao X, Yin F, Fu L, Ma Y, Ye L, Huang Y, Fan W, Gao W, Cai Y, Mou X. Garlic-derived exosome-like nanovesicles as a hepatoprotective agent alleviating acute liver failure by inhibiting CCR2/CCR5 signaling and inflammation. Biomaterials Advances. 2023;154:213592.
35. Liu J, Li W, Bian Y, Jiang X, Zhu F, Yin F, Yin L, Song X, Guo H, Liu J. Garlic-derived exosomes regulate PFKFB3 expression to relieve liver dysfunction in high-fat diet-fed mice via macrophage-hepatocyte crosstalk. Phytomedicine. 2023;112:154679.
36. Sundaram K, Teng Y, Mu J, Xu Q, Xu F, Sriwastva MK, Zhang L, Park JW, Zhang X, Yan J, et al. Outer Membrane Vesicles Released from Garlic Exosome-like Nanoparticles (GaELNs) Train Gut Bacteria that Reverses Type 2 Diabetes via the Gut-Brain Axis. Small. 2024;20(20):e2308680.
37. Xu J, Yu Y, Zhang Y, Dai H, Yang Q, Wang B, Ma Q, Chen Y, Xu F, Shi X, et al. Oral administration of garlic-derived nanoparticles improves cancer immunotherapy by inducing intestinal IFNγ-producing γδ T cells. Nat Nanotechnol. 2024;19(10):1569-78.
38. Ly NP, Han HS, Kim M, Park JH, Choi KY. Plant-derived nanovesicles: Current understanding and applications for cancer therapy. Bioact Mater. 2023;22:365-83.
39. Song H, Canup BSB, Ngo VL, Denning TL, Garg P, Laroui H. Internalization of Garlic-Derived Nanovesicles on Liver Cells is Triggered by Interaction With CD98. ACS Omega. 2020;5(36):23118-28.
40. Ou X, Wang H, Tie H, Liao J, Luo Y, Huang W, Yu R, Song L, Zhu J. Novel plant-derived exosome-like nanovesicles from Catharanthus roseus: preparation, characterization, and immunostimulatory effect via TNF-α/NF-κB/PU.1 axis. J Nanobiotechnol. 2023;21(1):160.
41. Li D, Tang Q, Yang M, Xu H, Zhu M, Zhang Y, Tian C, Nie Y, Wang J, Liang Y, et al. Plant-derived exosomal nanoparticles: potential therapeutic for inflammatory bowel disease. Nanoscale Adv. 2023;5(14):3575-88.
42. Yi C, Lu L, Li Z, Guo Q, Ou L, Wang R, Tian X. Plant-derived exosome-like nanoparticles for microRNA delivery in cancer treatment. Drug Deliv Transl Re. 2024;15(1):84-101.
43. Ghadami S, Dellinger K. The lipid composition of extracellular vesicles: applications in diagnostics and therapeutic delivery. Front Mol Biosci. 2023;10:1198044.
44. Lin F, Xu L, He Q, Chen Z, Zhang W, Tu J, Song Y, Zhong F, Lin S, Yang R, et al. Plant-derived nanovesicles as novel nanotherapeutics for alleviating endothelial cell senescence-associated vascular remodeling induced by hypertension. Pharmacol Res. 2025;214:107675.
45. Zhou Z, Li X, Liu J, Dong L, Chen Q, Liu J, Kong H, Zhang Q, Qi X, Hou D, et al. Honeysuckle-encoded atypical microRNA2911 directly targets influenza A viruses. Cell Res. 2014;25(1):39-49.
46. Qin Y, Zheng B, Yang G, Yang H, Zhou J, Yang Z, Zhang X, Zhao H, Shi J, Wen J. Salvia miltiorrhiza-Derived Sal-miR-58 Induces Autophagy and Attenuates Inflammation in Vascular Smooth Muscle Cells. Mol Ther Nucl Acids. 2020;21:492-511.
47. Xu X, Yuan T, Dad HA, Shi M, Huang Y, Jiang Z, Peng L. Plant Exosomes As Novel Nanoplatforms for MicroRNA Transfer Stimulate Neural Differentiation of Stem Cells In Vitro and In Vivo. Nano Lett. 2021;21(19):8151-59.
48. Cai H, Huang L, Hong R, Song J, Guo X, Zhou W, Hu Z, Wang W, Wang Y, Shen J, et al. Momordica charantia Exosome-Like Nanoparticles Exert Neuroprotective Effects Against Ischemic Brain Injury via Inhibiting Matrix Metalloproteinase 9 and Activating the AKT/GSK3beta Signaling Pathway. Front Pharmacol. 2022;13:908830.
49. Rongfeng Y, Fengxia L, Wenlin W, et al. Investigating the therapeutic effects and mechanisms of Carthamus tinctorius L.-derived nanovesicles in atherosclerosis treatment. Cell Commun Signal. 2024;22(1):178.
50. Shanthi KB, Pratiwi FW, Naillat F, Mammadova R, Sarpola M, Wu SH, Suokas M, Jokipii-Lukkari S, Kaisto S, Samoylenko A et al. Cloudberry-derived nanovesicles as stable oral drug delivery systems: gastrointestinal stability and age-related biodistribution in mice. Nanoscale. 2025; 17(36):21096-111.
51. Fang Z, Liu K. Plant-derived extracellular vesicles as oral drug delivery carriers. J Control Release. 2022, 350:389-400.

Alharbi KS, Fuloria NK, Fuloria S, Rahman SB, Al-Malki WH, Javed Shaikh MA, Thangavelu L, Singh SK, Rama Raju Allam VS, Jha NK, et al. Nuclear factor-kappa B and its role in inflammatory lung disease. Chem-Biol Interact. 2021;345:109568.

Zhang Z, Zhang C. Regulation of cGAS–STING signalling and its diversity of cellular outcomes. Nat Rev Immunol. 2025;25(6):425-44.